



## Article

# A New Fractional-Order Virtual Inertia Support Based on Battery Energy Storage for Enhancing Microgrid Frequency Stability

Morsy Nour <sup>1,2,\*</sup>, Gaber Magdy <sup>2,3</sup>, Abualkasim Bakeer <sup>4</sup>, Ahmad A. Telba <sup>5</sup>, Abderrahmane Beroual <sup>6</sup>, Usama Khaled <sup>2</sup> and Hossam Ali <sup>2</sup>

- <sup>1</sup> Institute for Research in Technology (IIT), ICAI School of Engineering, Comillas Pontifical University, 28015 Madrid, Spain
- <sup>2</sup> Department of Electrical Engineering, Faculty of Energy Engineering, Aswan University, Aswan 81528, Egypt; gabermagdy@aswu.edu.eg (G.M.); usamakhaled@energy.aswu.edu.eg (U.K.); hossam\_ali@energy.aswu.edu.eg (H.A.)
- <sup>3</sup> Faculty of Engineering, King Salman International University, El-Tor 46511, Egypt
- <sup>4</sup> Department of Electrical Engineering, Faculty of Engineering, Aswan University, Aswan 81542, Egypt
- <sup>5</sup> Electrical Engineering Department, College of Engineering, King Saud University, Riyadh 11421, Saudi Arabia; atelba@ksu.edu.sa
- <sup>6</sup> AMPERE Lab UMR CNRS 5005, Ecole Centrale de Lyon, University of Lyon, 36 Avenue Guy de Collongue, 69130 Ecully, France; abderrahmane.beroual@ec-lyon.fr
- \* Correspondence: mmohammed@comillas.edu

**Abstract:** Microgrids have a low inertia constant due to the high penetration of renewable energy sources and the limited penetration of conventional generation with rotating mass. This makes microgrids more susceptible to frequency stability challenges. Virtual inertia control (VIC) is one of the most effective approaches to improving microgrid frequency stability. Therefore, this study proposes a new model to precisely mimic inertia power based on an energy storage system (ESS) that supports low-inertia power systems. The developed VIC model considers the effect of both the DC-DC converter and the DC-AC inverter on the power of the ESS used. This allows for more precise and accurate modeling of the VIC compared to conventional models. Moreover, this study proposes a fractional-order derivative control for the proposed VIC model to provide greater flexibility in dealing with different perturbations that occur in the system. Furthermore, the effectiveness of the proposed fractional-order VIC (FOVIC) is verified through an islanded microgrid that includes heterogeneous sources: a small thermal power plant, wind and solar power plants, and ESSs. The simulation results performed using MATLAB software indicate that the proposed VIC scheme provides fast stabilization times and slight deviations in system frequency compared to the conventional VIC schemes. The proposed VIC outperforms the conventional load frequency control by about 80% and the conventional VIC model by about 45% in tackling load/RESs fluctuations and system uncertainty. Additionally, the studied microgrid with the proposed FOVIC scheme is noticeably more stable and responds faster than that designed with integer-order derivative control. Thus, the proposed FOVIC scheme gives better performance for frequency stability of low-inertia power systems compared to conventional VIC schemes used in the literature.

**Keywords:** fractional-order virtual inertia control; virtual inertia control; virtual synchronous generator; automatic generation control; battery energy storage; frequency regulation



**Citation:** Nour, M.; Magdy, G.; Bakeer, A.; Telba, A.A.; Beroual, A.; Khaled, U.; Ali, H. A New Fractional-Order Virtual Inertia Support Based on Battery Energy Storage for Enhancing Microgrid Frequency Stability. *Fractal Fract.* **2023**, *7*, 855. <https://doi.org/10.3390/fractalfract7120855>

Academic Editors: Arman Oshnoei and Behnam Mohammadi-Ivatloo

Received: 4 November 2023

Revised: 26 November 2023

Accepted: 28 November 2023

Published: 30 November 2023



**Copyright:** © 2023 by the authors. Licensee MDPI, Basel, Switzerland. This article is an open access article distributed under the terms and conditions of the Creative Commons Attribution (CC BY) license (<https://creativecommons.org/licenses/by/4.0/>).

## 1. Introduction

There is a worldwide interest in generating electricity from renewable energy sources (RESs). Various RESs are being integrated into power systems, such as hydro, solar, wind, geothermal, biomass, ocean energy, etc. Many countries aim to achieve more than 90% electricity generation from RESs by 2050 [1]. Energy security concerns, environmental

issues, and economic benefits drive this interest. However, the increase in intermittent RESs penetration results in tedious power system operation and control due to uncertainty and intermittency of RESs production [2].

Synchronous generators (SGs)-led conventional power systems have the inertia capability to maintain voltage and frequency deviations within standard ranges [3]. Though the decreasing inertia makes future power systems driven by power converters more susceptible to system insecurity [4]. Particularly for isolated small power systems and microgrids (MGs), the low-inertia feature adversely affects system stability when distributed generation (DG) penetration increases and loads suddenly change [5]. For instance, the abrupt rise in loads or disconnection of generation units may exacerbate the transient response of MGs, such as the rate of change of frequency (RoCoF) and frequency deviation, leading to system instability [6], and protection devices such as under-frequency load shedding may intervene to prevent a blackout of the whole MG [7]. Many studies investigated the frequency control of microgrids integrated with a high share of RESs [8,9].

Various secondary controllers were developed in previous studies to improve power systems' frequency stability in addition to conventional controllers. The proportional integral derivative derivative (PIDDD) controller optimized by the fruit fly algorithm provided better performance than the integral (I), proportional integral (PI), proportional integral derivative (PID), and integral derivative derivative (IDD) controllers for a deregulated power system [10]. The frequency stability of a two-area power system is improved using a new cascaded controller optimized using artificial rabbit optimizers [11]. The authors of [12] enhanced islanded MG frequency stability using a prairie dog optimization-based cascaded controller. Reference [13] used a new cascaded controller optimized by Barnacle Mating Optimizer for improving the frequency stability of two-area interconnected MGs. Another study used a fuzzy cascaded controller to improve frequency control of an islanded MG containing several types of generators and energy storage [14].

In an attempt to cope with the lack of inertia concern, virtual synchronous generators (VSGs) or virtual inertia concepts are proposed [15–18]. With the aid of these techniques, the power electronic devices coupled with RESs or energy storage systems (ESSs) are controlled to emulate the real SGs swing equation and deliver the necessary inertia support to the grid. Consequently, the system frequency stability could be improved, and the frequency fluctuations and RoCoF were reduced following disturbances [19].

Several control techniques have been developed in the literature based on the virtual inertia concept. A conventional PI approach has been applied in [20] to enhance the dynamic security of isolated MGs. Furthermore, a PI-based virtual inertia control (VIC) of a wind turbine has been implemented [21]. In [22], a fuzzy-based virtual inertia strategy is introduced to control frequency deviation in a hybrid power system. Methodologies considering robust control techniques, such as the coefficient diagram method and  $H_\infty$  have been proposed in [23,24] for MGs considering high RESs penetration. Other methodologies have adopted model predictive control [25] and adaptive VIC [26,27] to improve system frequency stability.

To attain the best performance from the above-mentioned controllers, they usually contain parameters that need to be optimally fine-tuned. However, selecting the optimal parameters for various virtual inertia frequency controllers in MGs is challenging, as it either employs trial-and-error methods or depends on the designer's experience. To determine the optimal frequency controller parameters, many researchers have implemented a variety of optimization techniques, including particle swarm optimization [28], a modified gray wolf optimization algorithm [29], a chaotic crow search algorithm [30], a Newton-based eigenvalue optimization algorithm [31], a knee point-driven evolutionary algorithm [32], a jellyfish search optimizer [33], and other recently developed optimization algorithms that have been successfully implemented in frequency control applications.

It can be noticed from the literature that the adoption of virtual inertia increases the system order, which causes the output active power to oscillate and adversely affects frequency dynamics. In addition, in the scope of fine-tuning the prior controllers, it is

not easy to realize a reasonable trade-off in performance between robustness and control. Hence, it is challenging to guarantee robust stability and efficiency with the aforementioned controlling approaches under a wide range of demand and generation perturbations.

In recent days, the fractional-order (FO) controller has received a lot of attention due to its greater flexibility for adjusting system dynamics, specifically for systems operating in uncertain environments [34–36]. It has been adopted in a deregulated environment for automatic generation control (AGC) [37] and load frequency control (LFC) [38]. The FO controller's superiority is due to its two additional tuning knobs, such as the FO of the differentiator ( $\mu$ ) and the integrator ( $\lambda$ ). Because of their inherent flexibility, several researchers have recommended FO controllers over traditional PI and PID controllers for power system stability applications [39,40]. On the other hand, rare work has considered the application of FO derivative in VIC (FOVIC) to improve the conventional VIC (i.e., which uses integer order derivative) response, as in [41,42]. This new concept needs further study on different power systems with different resources and operating conditions. Interestingly, the FOVSG was created in [41,42] with the presumption that the DC link is ideal; nevertheless, the DC link's energy storage has to be further included in the VIC model due to its limitations. In addition, the authors of [41,42], did not study the influence of variation of the virtual inertia constant with different values of FO operators.

Inspired by the above considerations, this work proposes a FOVIC that is applied to an islanded MG, including a small thermal power plant, wind power plant, solar power plants, ESS, and MG loads. The contributions of this research are summarized as follows:

1. Develop a new VIC model separating the DC-DC converter and DC-AC inverter stages. This allows for more precise and accurate modeling of the individual stages compared to the conventional VIC model introduced in [4,20,25,27].
2. Propose a FO derivative control that is applied to the suggested, developed virtual inertia model. The FOVIC has the benefit of reducing system order, which can considerably suppress frequency fluctuation and output power oscillation.
3. Including FOVIC boosts the system's degree of freedom, thus strengthening system stability and further enhancing dynamic performance in the presence of numerous operational circumstances and high RES penetration rates.
4. The considered islanded MG with the proposed FOVIC scheme is examined under different values of the virtual inertia constant and different values of FO operators, highlighting the best operating values for varied case studies.
5. Graphical and numerical outcomes from simulation indicate how competent the suggested control strategy is, where it can significantly reduce frequency deviations compared to the conventional controllers in the literature.

The rest of this paper is structured as follows: Section 2 introduces system configuration. In Section 3, the design of the proposed FOVIC control system is developed. Section 4 verifies the effectiveness of the suggested model and FOVIC through simulation results. The discussion is presented in Section 5. In Section 6, this paper's main conclusions are summarized.

## 2. System Modelling and Configuration

This study uses an islanded MG system, i.e., a test system, to examine the effectiveness of the proposed VIC model and the impact of the FO control strategy on its performance. The studied MG includes a dispatchable distributed generator (i.e., small thermal power plant), non-dispatchable distributed generators (i.e., wind and solar power plants), ESS, and MG loads [20]. Moreover, the studied system contains a 20 MW thermal power plant, a 4 MW solar power plant, an 8 MW wind power plant, a 1 MW ESS, and 15 MW local loads. The studied island, MG, has a 20 MW power base. A schematic diagram of the investigated system with the proposed control strategy is revealed in Figure 1. Figure 2 shows the frequency response model of the studied system with the proposed developed control strategy, and the studied system's parameters are given in Table 1.

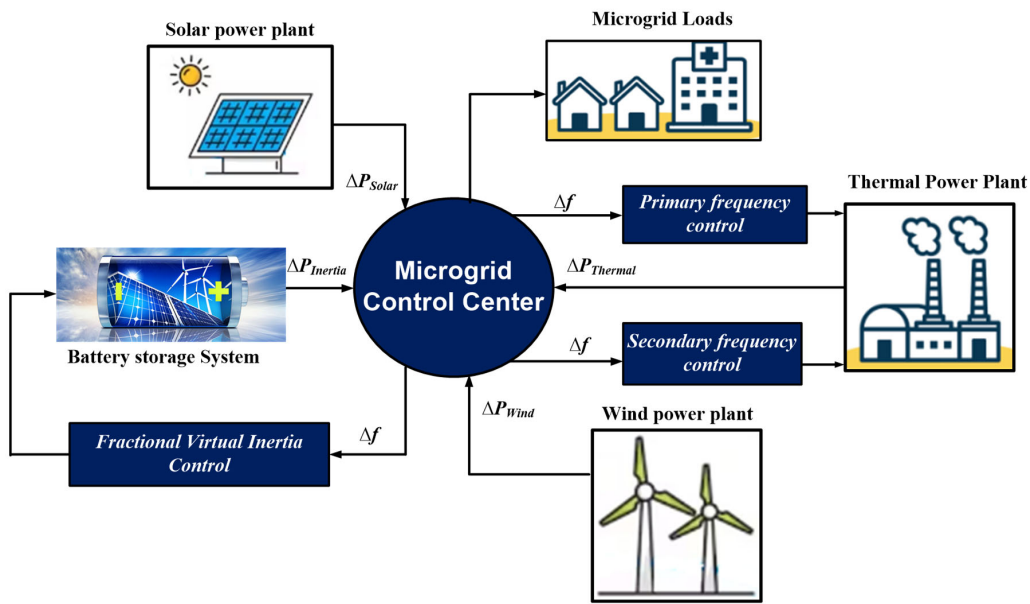


Figure 1. A schematic diagram of the studied islanded MG with the proposed FOVIC strategy.

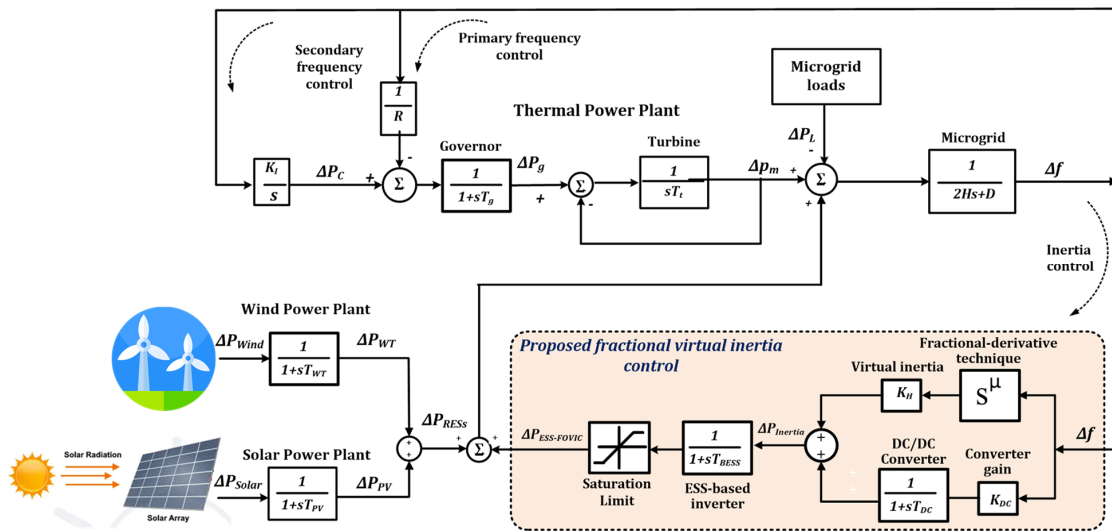


Figure 2. A LFC model of the studied islanded MG with the proposed developed FOVIC.

Table 1. Values of the studied MG parameters [20].

Parameter	Value
Equivalent inertia constant, $H$ (p.u. MWs)	0.082
Microgrid frequency, $f$ (Hz)	50.000
Microgrid damping coefficient, $D$ (p.u.MW/Hz)	0.015
Turbine time constant, $T_t$ (s)	0.400
Governor time constant, $T_g$ (s)	0.100
Speed droop characteristic, $R$ (Hz/p.u.MW)	2.400
Integral control variable gain, $K_I$	-0.50
Wind turbine time constant, $T_{WT}$ (s)	1.500
Solar system time constant, $T_{PV}$ (s)	1.800
Inverter time constant for conventional VIC, $T_{BESS}$ (s)	0.200
Inverter time constant for proposed VIC, $T_{BESS}$ (s)	0.100
DC/DC converter time constant, $T_{DC}$ (s)	0.100
DC/DC converter gain, $K_{DC}$	1.000

The fifth-order linearized system for the islanded MG, which considers high penetration of RESs, can be effectively modeled using the state-space approach. The deviation of the examined system’s frequency can be obtained by considering the governor action (i.e., the primary control loop) and the LFC (i.e., the secondary control loop), as follows:

$$\dot{\Delta f} = \frac{1}{2H}(\Delta P_m + \Delta P_{WT} + \Delta P_{PV} - \Delta P_L) - \frac{D}{2H} * \Delta f \tag{1}$$

where,

$$\Delta \dot{P}_g = -\frac{1}{T_g}(\Delta P_g) - \frac{1}{R.T_g} * \Delta f + \frac{1}{T_g}(\Delta P_C) \tag{2}$$

$$\Delta \dot{P}_m = -\frac{1}{T_t}(\Delta P_m) + \frac{1}{T_t}(\Delta P_g) \tag{3}$$

$$\Delta \dot{P}_{WT} = \frac{1}{T_{WT}}(\Delta P_{Wind}) - \frac{1}{T_{WT}}(\Delta P_{WT}) \tag{4}$$

$$\Delta \dot{P}_{PV} = \frac{1}{T_{PV}}(\Delta P_{Solar}) - \frac{1}{T_{PV}}(\Delta P_{PV}) \tag{5}$$

In this study, the power changes caused by the wind ( $\Delta P_{Wind}$ ), solar ( $\Delta P_{Solar}$ ), and load ( $\Delta P_L$ ) are taken into account as disturbance signals. Using the state variables from (1) to (5), the linearized state-space model of the investigated MG could be easily developed as follows:

$$\dot{X} = AX + BU + EW \tag{6}$$

$$Y = CX + DU + ZW \tag{7}$$

where,

$$X^T = [\Delta f \quad \Delta P_g \quad \Delta P_m \quad \Delta P_{WT} \quad \Delta P_{PV}]$$

$$W^T = [\Delta P_{Wind} \quad \Delta P_{Solar} \quad \Delta P_L]$$

$$Y = [\Delta f]$$

where  $W$  is the input perturbation vector,  $U$  is the control input signal,  $X$  is the state vector, and  $Y$  is the control output signal.  $A$  is the state matrix of the studied system.  $B$  and  $E$  correspond to the control input signal and the disturbance inputs. The output measurement, or input to the load-frequency controller, is represented by  $C$ .  $D$  and  $Z$  are zero vectors with the same size as the input control signal and disturbance vector, respectively. As a result, the islanded MGs complete state-space representation, taking into account RESs, can be obtained in Equations (8) and (9).

$$\dot{X} = \begin{bmatrix} -\frac{D}{2H} & 0 & \frac{1}{2H} & \frac{1}{2H} & \frac{1}{2H} \\ -\frac{1}{RT_g} & -\frac{1}{T_g} & 0 & 0 & 0 \\ 0 & \frac{1}{T_t} & -\frac{1}{T_t} & 0 & 0 \\ 0 & 0 & 0 & -\frac{1}{T_{WT}} & 0 \\ 0 & 0 & 0 & \frac{1}{T_{WT}} & -\frac{1}{T_{PV}} \end{bmatrix} * \begin{bmatrix} \Delta f \\ \Delta P_g \\ \Delta P_m \\ \Delta P_{WT} \\ \Delta P_{PV} \end{bmatrix} + \begin{bmatrix} 0 \\ \frac{1}{T_g} \\ 0 \\ 0 \\ 0 \end{bmatrix} * [\Delta P_C] + \begin{bmatrix} 0 & 0 & -\frac{1}{2H} \\ 0 & 0 & 0 \\ 0 & 0 & 0 \\ \frac{1}{T_{WT}} & \frac{1}{T_{PV}} & 0 \\ 0 & 0 & 0 \end{bmatrix} * \begin{bmatrix} \Delta P_{Wind} \\ \Delta P_{Solar} \\ \Delta P_L \end{bmatrix} \tag{8}$$

$$Y = [1 \quad 0 \quad 0 \quad 0 \quad 0] X + [0] U + \begin{bmatrix} 0 & 0 & 0 \\ 0 & 0 & 0 \\ 0 & 0 & 0 \\ 0 & 0 & 0 \\ 0 & 0 & 0 \end{bmatrix} W \tag{9}$$

### 3. Proposed Fractional-Order VIC (FOVIC)

#### 3.1. Description of the Fractional-Order Calculus

Despite being proposed 300 years ago, the utilization of FO has only recently become prevalent due to its complexity [36]. Generic integral and differential notations into any actual number are possible by means of the fractional operators in the controller. The FO differentiator is a mathematical operator that can be viewed as a more generalized form of integral and differential operators, as indicated in the following way:

$$D_{lb,ub}^q = \begin{cases} \frac{d^q}{dt^q} & q > 0 \\ 1 & q = 0 \\ \int_{lu}^{ub} (d\tau)^{-q} & q < 0 \end{cases} \tag{10}$$

where  $q$  is the FO operator and  $ub$  and  $lb$  are the upper and lower bands to calculate operator  $D$ .

Two different theories can define the FO principle. The Riemann-Liouville (RL) method is the original one and is utilized to identify the order derivative of a function  $f(t)$  [41,42] as follows:

$$D_{lb,ub}^q f(t) = \frac{1}{\Gamma(n-q)} \left(\frac{d}{dt}\right)^n \int_{lb}^{ub} \frac{f^n(\tau)}{(t-\tau)^{q-n+1}} d\tau \tag{11}$$

where  $\Gamma(z) = \int_0^\infty t^{z-1} e^{-t} dt, \Re(z) > 0$  is the function of Gamma,  $n \in \mathbb{N}$  and the variable  $q$  is limited as  $n-1 < q < n$ .

The previous fractional derivative of RL in (11) can then be transformed using the well-known Laplace method as follows [43]:

$$\mathcal{L}\{D_0^q f(t)\} = s^q F(s) - \sum_{y=0}^{n-1} s^y \left(D_0^{q-y-1} f(t)\right)|_{t=0} \tag{12}$$

where  $s$  is the Laplace operator.

The second definition related to the essential notation of FO is Caputo’s definition, where the time-domain representation for  $q$  order of a function  $f(t)$  can be stated as follows:

$$D_{lb,ub}^q f(t) = \begin{cases} \frac{1}{\Gamma(n-q)} \left(\int_{lb}^{ub} \frac{f^n(\tau)}{(t-\tau)^{1-n+q}} d\tau\right) & n-1 < q < n \\ \left(\frac{d}{dt}\right)^n f(t) & q = n \end{cases} \tag{13}$$

Once more, we apply the Laplace transformation to Equation (13) to result in Equation (14), which has an initial condition and represents the integral order with a specific physical significance.

$$\mathcal{L}\{D_0^q f(t)\} = s^q F(s) - \sum_{k=0}^{n-1} s^{q-k-1} f^{(k)}(0) \tag{14}$$

The implementation of FO operators in the time domain involves complicated mathematical calculations. The recursive estimation method is typically used to implement the FO definition [44]. The Laplace transformation of the  $q^{th}$  derivative is as follows:

$$s^q \approx K \prod_{k=-N}^N \frac{s + \omega'_k}{s + \omega_k} \tag{15}$$

where

$$K = \omega_h^q$$

$$\omega'_k = \omega_b \left(\frac{\omega_h}{\omega_b}\right)^{\frac{k+N+(1-q)/2}{2N+1}}$$



$$\omega_k = \omega_b \left( \frac{\omega_h}{\omega_b} \right)^{\frac{k+N+(1+q)/2}{2N+1}}$$

$N$  is an effective frequency range approximation order  $[\omega_b, \omega_h]$  that can be chosen as  $[-1000, 1000]$  rad/s.

The fractional calculus expands on the conventional PID controller by allowing more variables to be adjusted. Unlike the traditional PID controller, which only has three variables that can be fine-tuned, the FOPID controller provides five variables for tuning. Consequently, there are two additional variables of integral and differential FOs  $\lambda$  and  $\mu$ , respectively, as shown in Figure 3. When compared with the conventional PID, these variables have the capability to improve the controller’s stability, transient time, and steady-state error. Moreover, it offers the controller greater flexibility and enables them to manage disturbances in the system that occur across a broad range of The transfer function of the FOPID controller is fully represented below:

$$G_c(s) = K_P + K_I \left( \frac{1}{s} \right)^\lambda + K_D s^\mu \tag{16}$$

where  $\lambda$  and  $\mu$  lie in the range of 0 and 1, which can decrease the steady-state error and rise time in the system.

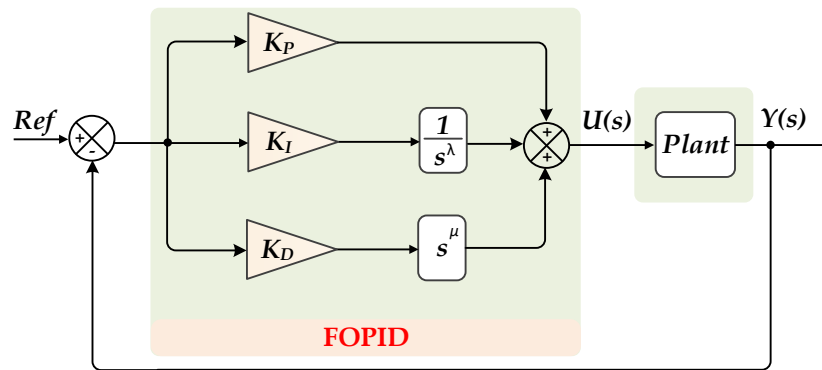


**Figure 3.** The basic structure of the FOPID controller as an example of applying FO calculus.

### 3.2. Description of the Proposed Fractional-Order Virtual Inertia Control

The FO controller-based PID has been widely applied for power system stability due to its wide stability and robustness. In contrast, most of the studies are dedicated to LFC [38,45], and AGC [40]. In all prior work in the literature, the notion of FOPID is used as a controller to support the LFC. The synchronous generator, which is regarded as the principal dynamic source of the conventional power system, contributes inertia to the grid via its rotating mass in the traditional power system [46], as in (17).

$$H = \frac{\sum_{x=1}^G H_x S_{B,x}}{S_B} \tag{17}$$

where  $G$  denotes the whole number of generating units coupled to the grid,  $S_B$  is the power system’s rated capacity, and  $H_x$  and  $S_{B,x}$  are the inertia value and rated power of the generation units, respectively. Moreover, the swing equation can be employed to explain the rotating dynamics of actual synchronous machines, as in (18).

$$\Delta P_M(s) - \Delta P_L(s) = (2Hs + D)\Delta f(s) \tag{18}$$

where  $\Delta P_M$  is the change in mechanical power,  $\Delta P_L$  is the load power change, and  $\Delta f$  is the frequency deviation.

To enhance the stability of low system inertia in the presence of a significant amount of RESs, it is possible to recreate the synthetic damping attribute and synthetic inertia power in the power system. This action can effectively improve the frequency stability of the power system. Thus, the inverter-based ESS, which is used to inject/absorb active power into/from the power system, is regulated based on the VIC, as in (19).

$$\Delta P_{VIC} = K_H s * \Delta f \tag{19}$$

where  $K_H$  is the virtual inertia constant of the VIC.

The typical VIC system on the basis of battery ESS (BESS) is shown in Figure 4, which simulates the real synchronous generator’s inertia. When the RESs are penetrated, the VIC-based ESSs dynamic equation that reflects the power system’s desired power can be stated as in (20). The amount of power that the inertia of the BESS can generate is constrained by two factors: the maximum capacity of the BESS during the processes of charging and discharging, and the state of charge (SOC) of the BESS. These limitations prevent the inertia output power from exceeding the rated capacity of the BESS and avoid the lifetime degradation of the battery.

$$\Delta P_{ESS-VIC} = \frac{K_H s}{1 + sT_{BESS}} (\Delta f) \tag{20}$$

where  $T_{BESS}$  refers to the inverter-based BESS time constant.

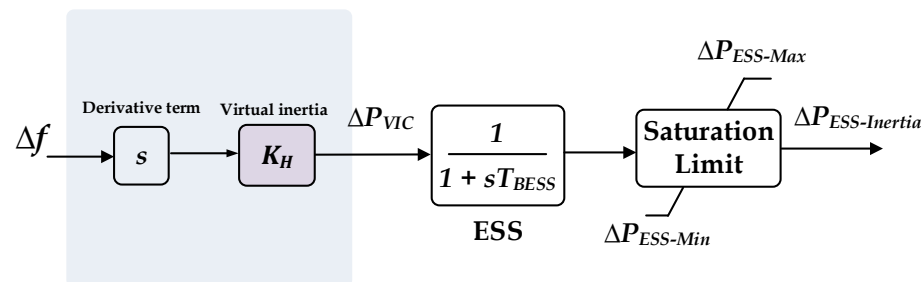


Figure 4. The dynamic structure of conventional VIC-based ESS.

The proposed VIC model separates the DC-DC converter stage and the DC-AC inverter stage, as shown in Figure 5. Each stage is represented by a first-order model with different time constants ( $T_{DC}$  for the DC-DC converter and  $T_{BESS}$  for the DC-AC inverter) and conversion gains ( $K_{DC}$  for the DC-DC converter and unity for the DC-AC inverter). This allows for more precise and accurate modeling of the individual stages. Typically, when the inertia power is not being emulated, the base power of the BESS is directly proportional to the deviation in frequency. This relationship can be represented mathematically as:

$$\Delta P_{ESS} = \Delta f \times \frac{K_{DC}}{1 + sT_{DC}} \times \frac{1}{1 + sT_{BESS}} \tag{21}$$

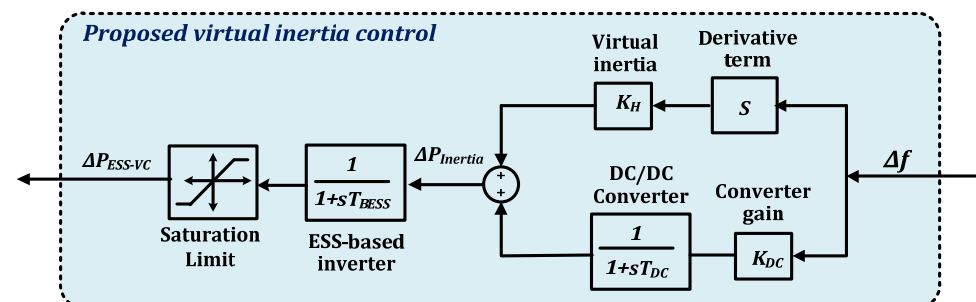


Figure 5. The proposed VIC-based ESS dynamic structure.



The complete transfer function of the proposed VIC can be expressed as follows:

$$\Delta P_{ESS-VIC} = \Delta f \times \left( \frac{K_{DC}}{1 + sT_{DC}} + K_H s \right) \times \frac{1}{1 + sT_{BESS}} \tag{22}$$

where  $K_H$  is the virtual inertia constant.

Moreover, this study intends to show how the order of the derivative term of the inertia term can influence the power system’s maximum frequency deviation, as shown in Figure 6. After analyzing Figure 6, it can be concluded that the optimal order of the  $s$  operator is 0.4. This value is crucial as it ensures the minimum frequency deviation is achieved at various points of  $K_H$ . In other words, the  $s$  operator plays a significant role in maintaining stability and consistency in the system’s frequency response. As we already indicated, the FO controller typically served as the secondary controller in most prior work. The FOVIC has the significant advantage of minimizing the system’s order, leading to a substantial decrease in frequency fluctuations and output power oscillations. The complete structure of the proposed FOVIC is shown in Figure 7.

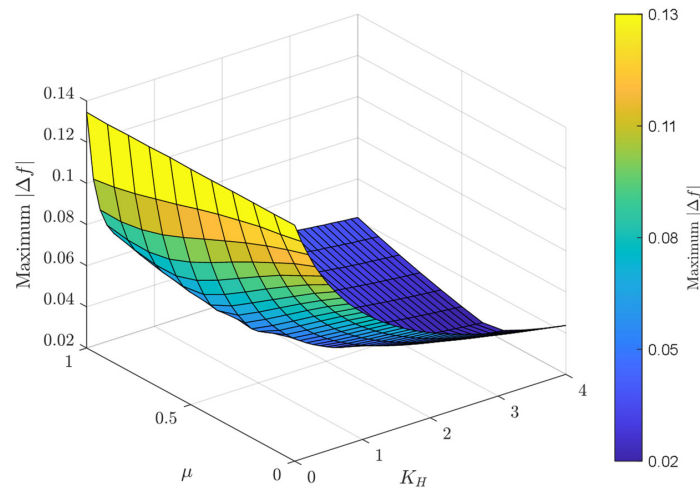


Figure 6. Effect of the virtual inertia constant and FO operator on the system frequency deviation.

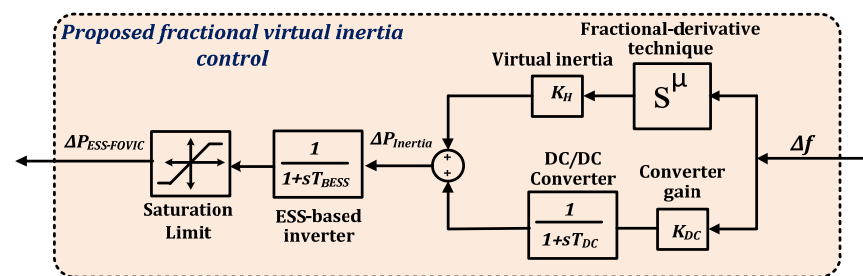


Figure 7. The proposed FOVIC to support the dynamic stability of MG.

The proposed FOVIC will undergo a second modification compared to Figure 4, which involves replacing the entire order of the inertial emulation with a fractional order. To achieve this, the output power and its sign will be combined with the required power from the DC-DC stage. The resulting power will then be set as a command for the inverter to supply power to the power system. The complete transfer function of the proposed FOVIC can be expressed as in (23):

$$\Delta P_{ESS-FOVIC} = \Delta f \times \left( \frac{K_{DC}}{1 + sT_{DC}} + K_H s^\mu \right) \times \frac{1}{1 + sT_{BESS}} \tag{23}$$

where  $\mu$  is the order of the inertia derivative.

#### 4. Simulation Results

To simulate the researched MG, a MATLAB/Simulink program is employed. With the proposed developed VIC model, which is depicted in Figure 2, and the system's parameters listed in Table 1 [20], the simulation results have been extracted based on two case studies, as follows:

- A. Validate the proposed developed VIC model's superiority compared with the conventional known VIC model, which is presented in many studies, e.g., [2,8,9,12,14,16].

Impact of the FO derivative on the developed structure of the suggested VIC model Both case studies are investigated through different scenarios under various situations of RES, load variation, and system inertia changes, as follows:

##### A1. Evaluation of the developed VIC model's performance under sudden load changes and different values of the virtual inertia constant

In this case, the suggested developed VIC scheme is compared with both the known conventional VIC scheme and without VIC (i.e., using conventional frequency control only) in the studied islanded MG under different values of virtual inertia constant as well as a 10% step change in load that occurs at time = 0 s. Figure 8 and Table 2 exhibit the frequency deviation of the investigated system with diverse control techniques under the nominal system parameters. From this simulation result, the studied MG with the suggested developed VIC scheme is noticeably more stable and quicker than the conventional VIC scheme. Moreover, the studied system with conventional frequency control (i.e., without the VIC scheme) has high overshoots and slow responses compared to the case of the proposed developed VIC scheme. In contrast, although the frequency deviation of the system with VIC schemes (i.e., the proposed and conventional schemes) is more suppressed when the  $K_H$  value is increased, the system with the known conventional VIC needs more time to achieve stability. Thus, by applying the proposed developed VIC scheme, the dynamic stability of the studied MG considering different values of  $K_H$  has been preserved.

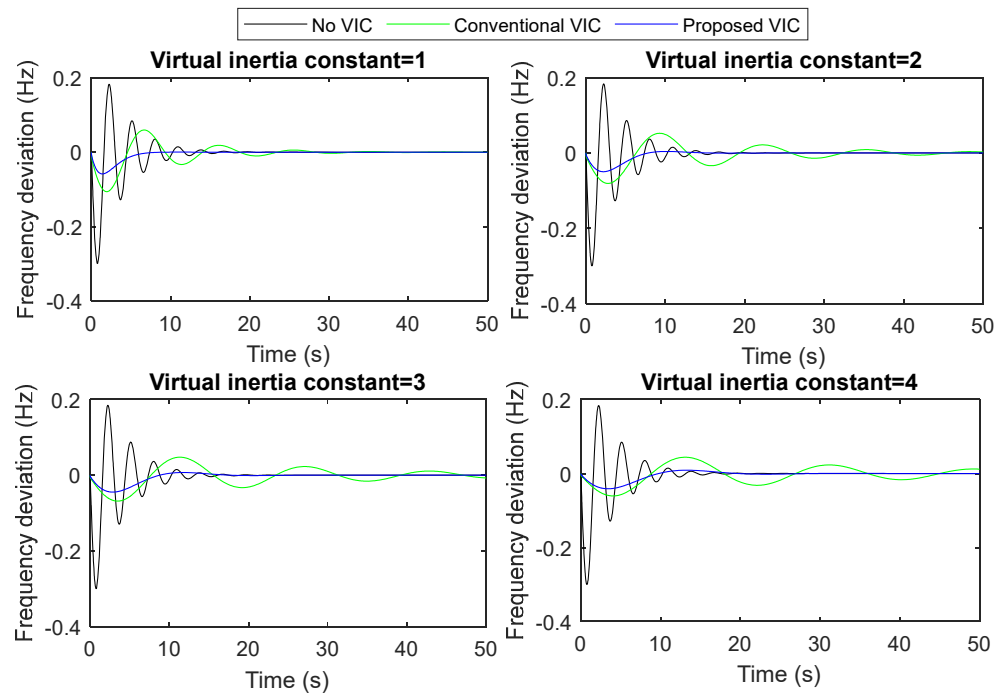


Figure 8. The frequency response of the MG with different values of  $K_H$  for case A1.

**Table 2.** Values of performance indices for case A1.

Control Approach	$\Delta f (K_H = 1)$			$\Delta f (K_H = 2)$			$\Delta f (K_H = 3)$			$\Delta f (K_H = 4)$		
	MUS (Hz)	MOS (Hz)	$T_S$ (s)	MUS (Hz)	MOS (Hz)	$T_S$ (s)	MUS (pu)	MOS (pu)	$T_S$ (s)	MUS (pu)	MOS (pu)	$T_S$ (s)
No VIC	$2.99 \times 10^{-1}$	$1.82 \times 10^{-1}$	28.72	$2.99 \times 10^{-1}$	$1.82 \times 10^{-1}$	28.72	$2.99 \times 10^{-1}$	$1.82 \times 10^{-1}$	28.72	$2.99 \times 10^{-1}$	$1.82 \times 10^{-1}$	28.72
Con. VIC	$1.06 \times 10^{-1}$	$5.96 \times 10^{-2}$	63.74	$8.08 \times 10^{-2}$	$5.24 \times 10^{-2}$	108.37	$6.84 \times 10^{-2}$	$4.75 \times 10^{-2}$	155.06	$6.06 \times 10^{-2}$	$4.40 \times 10^{-2}$	204.26
Pro. VIC	$5.85 \times 10^{-2}$	$1.05 \times 10^{-4}$	13.09	$4.97 \times 10^{-2}$	$4.15 \times 10^{-3}$	22.41	$4.47 \times 10^{-2}$	$7.06 \times 10^{-3}$	33.81	$4.13 \times 10^{-2}$	$8.87 \times 10^{-3}$	46.07

**A2. Evaluation of the developed VIC model’s performance under several load step changes**

In this case, a series of sudden load changes are applied in the investigated MG system with varied values of the virtual inertia. The step load change during the period of the simulation is revealed in Figure 9. Figure 10 demonstrates the frequency deviation of the studied MG with different control techniques under this disturbance. The results prove that the suggested developed VIC scheme gives the best performance for the studied islanded MG compared to the other control techniques, and the MG frequency variations are kept within the recommended levels during the load changes. Regarding the use of different values of the virtual inertia constant, the proposed developed VIC scheme showed fast stabilization time and slight deviations in system frequency compared to the conventional VIC scheme, which needs more time to stabilize.

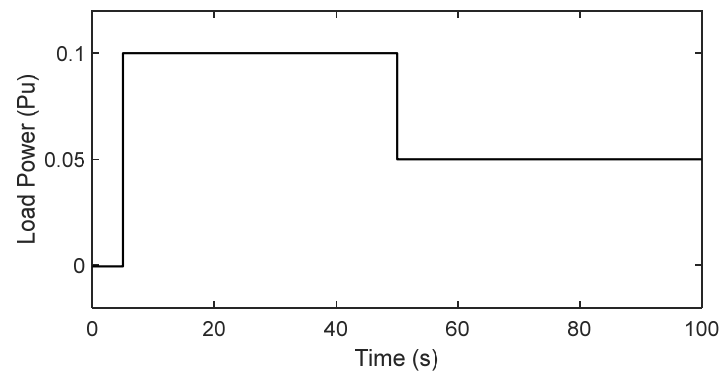


**Figure 9.** Load step change for case A2.

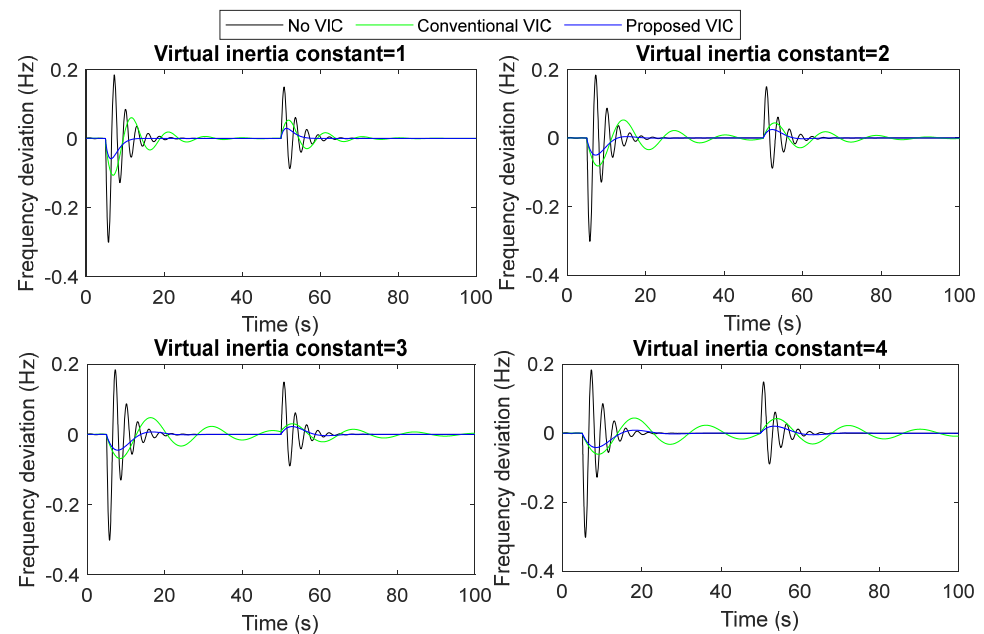


**Figure 10.** The frequency response of the MG with different values of  $K_H$  for case A2.

### A3. Evaluation of the developed VIC model's performance under step load change and RES presence

In this case, the MG with the suggested developed VIC scheme is studied under the following operational circumstances: a series of abrupt load changes shown in Figure 11 and power fluctuations of the RESs depicted in Figure 12. Figure 13 shows the frequency response of MG with the different control schemes, considering different values of virtual inertia. Figure 13 shows that the considered islanded MG with the suggested developed VIC scheme is more efficient and dependable. Additionally, in comparison with the conventional VIC scheme, the suggested scheme results in a better frequency response throughout all disturbances and operating conditions of the MG. On the other hand, conventional frequency control (i.e., without the VIC scheme) provided the poorest performance with high values of frequency deviation. Hence, with the proposed developed VIC scheme, the islanded MG system's overall performance is at its finest.

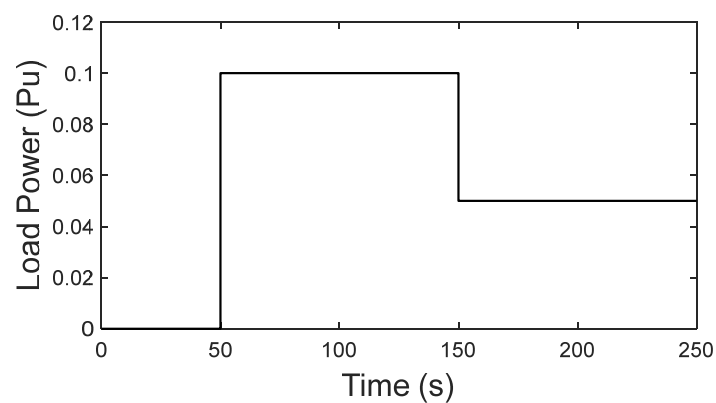


Figure 11. Load step change for case A3.

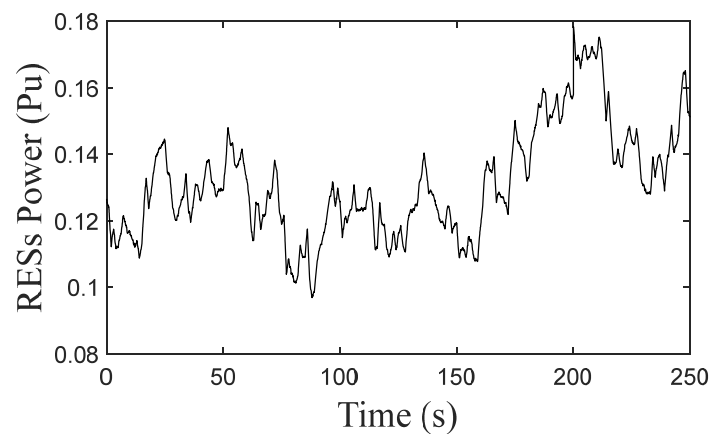
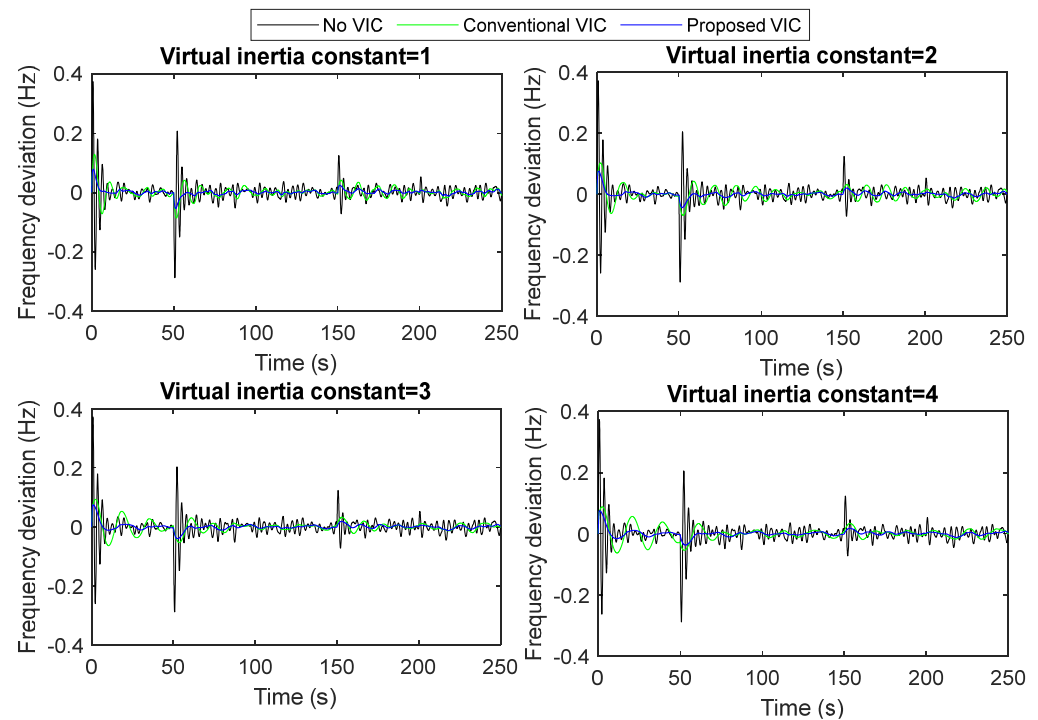


Figure 12. Renewables power generation profile for case A3.



**Figure 13.** The frequency response of the MG with RES generation and different values of  $K_H$  for case A3.

#### A4. Evaluation of the developed VIC model's performance considering communication delay.

Communication time delays are widely acknowledged in control systems for their potential to diminish system performance and induce instability. Consequently, these delays pose a significant challenge, emerging as a noteworthy uncertainty in analyzing the frequency stability of the power systems, given their ongoing expansion and increasing complexity. The effect of the communications delays with the proposed VIC strategy is tested at different time delays, as shown in Figures 14 and 15. This test considers both the communication time delay affecting the control input (i.e., before the LFC) and the delay in the control action (i.e., after the LFC). The effectiveness of the proposed VIC is evident, as it results in a lower frequency deviation compared to both the conventional VIC strategy and the LFC without VIC implementation. Additionally, with the proposed VIC, the system frequency achieves steady-state more rapidly than with the other two strategies. Notably, as the time delay increases from 0.1 s in Figure 14 to 0.2 s in Figure 15, both the conventional VIC and no VIC strategies exhibit heightened overshoot and settling time in frequency deviations. Consequently, applying the proposed VIC effectively mitigates the impact of communication delays without compromising the system's stability.

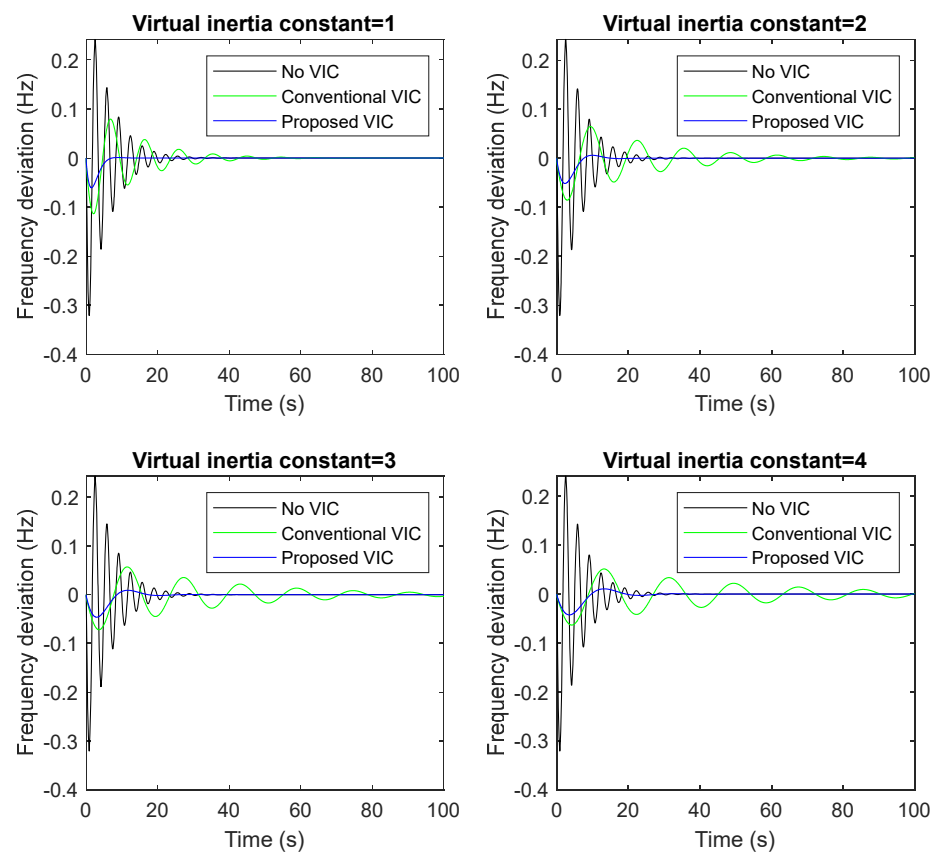


**Figure 14.** Effect of the 0.1 s communications delay before and after LFC on the MG frequency response for case A4.

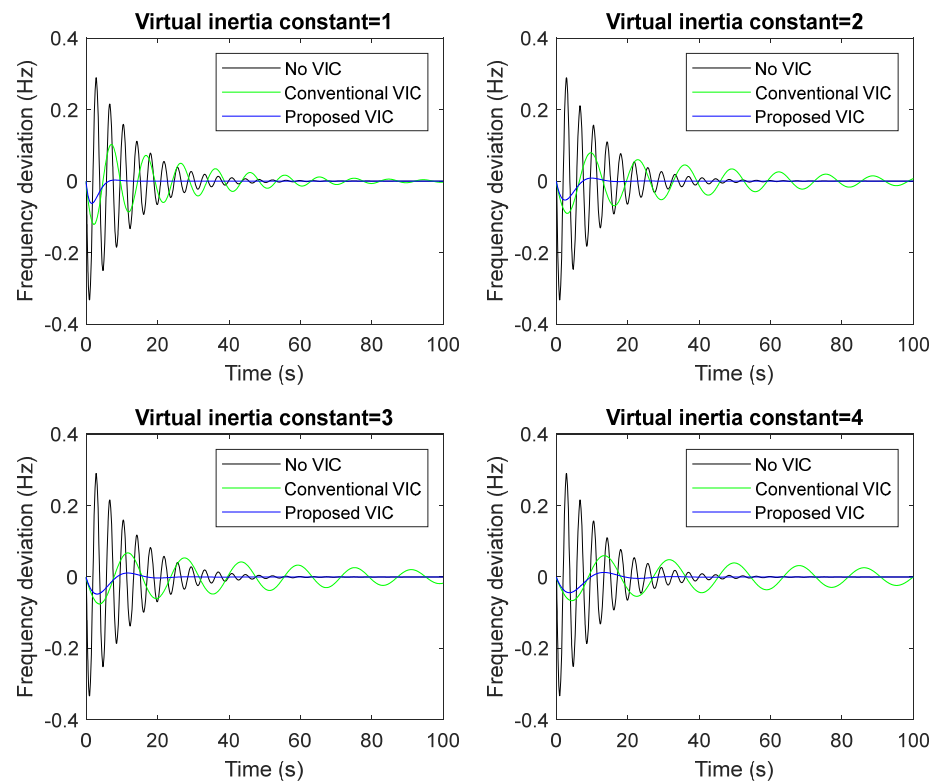


**Figure 15.** Effect of the 0.2 s communications delay before and after LFC on the MG frequency response for case A4.



### B1. Evaluation of the proposed FOVIC model’s performance under sudden load change

In this case, the impact of the FO control technique has been considered in the suggested structure of the developed VIC scheme. Therefore, the MG with the suggested FOVIC scheme is examined under different values of virtual inertia constant, different values of FO operators ( $\mu$ ) (i.e., 0.2, 0.4, 0.6, 0.8, and 1), and a 10% step change in load that occurs at time = 0 s. Figure 16 and Table 3 display the frequency deviation of the investigated system with FOVIC under the nominal system parameters. From Figure 16, it is clear that the higher the value of  $K_H$ , the more the MG with the proposed FOVIC can dampen the frequency deviations, but it needs more time to achieve stability. On the other side, the role of the FO operator in the suggested FOVIC is shown to change the system’s dynamic performance with respect to the overshoot, undershoot, and settling time. Therefore, the results indicate that the MG with the suggested FOVIC scheme at the fractional operator ( $\mu$ ) equals 0.4 is noticeably more stable and quicker than that designed with other fractional operator values. Moreover, it is obvious that this value is consistent with the range of values previously mentioned in the theoretical analysis section.

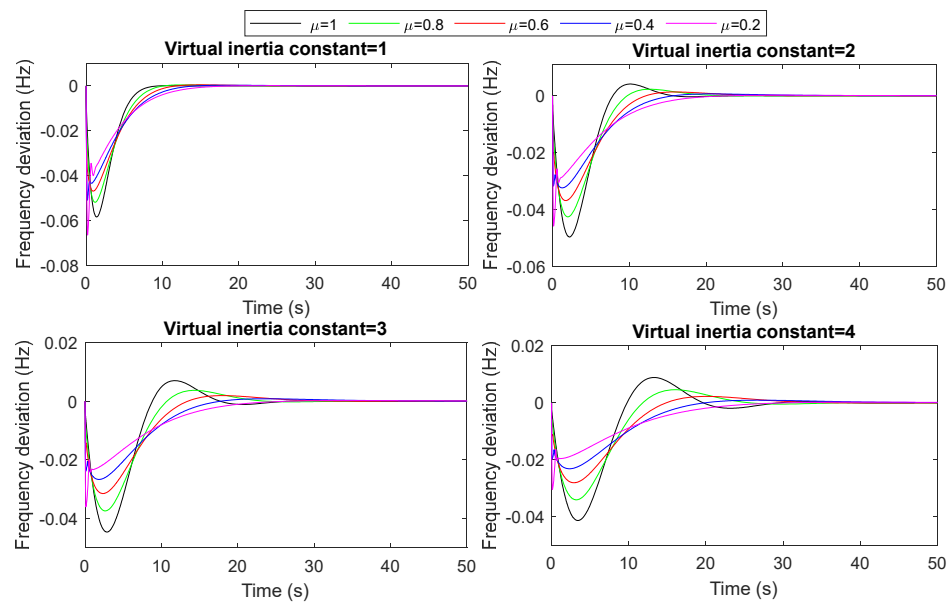


Figure 16. The frequency response of the MG with different values of  $K_H$  and fractional operators for case B1.

Table 3. Values of performance indices for case B1.

FO Operator	$\Delta f (K_H = 1)$			$\Delta f (K_H = 2)$			$\Delta f (K_H = 3)$			$\Delta f (K_H = 4)$		
	MUS (Hz)	MOS (Hz)	$T_S$ (s)	MUS (Hz)	MOS (Hz)	$T_S$ (s)	MUS (pu)	MOS (pu)	$T_S$ (s)	MUS (pu)	MOS (pu)	$T_S$ (s)
$\mu=1$	$5.85 \times 10^{-2}$	$1.05 \times 10^{-4}$	13.09	$4.97 \times 10^{-2}$	$4.15 \times 10^{-3}$	22.41	$4.47 \times 10^{-2}$	$7.06 \times 10^{-3}$	33.81	$4.13 \times 10^{-2}$	$8.87 \times 10^{-3}$	46.07
$\mu=0.8$	$5.19 \times 10^{-2}$	$4.78 \times 10^{-4}$	22.44	$4.26 \times 10^{-2}$	$2.32 \times 10^{-3}$	22.11	$3.75 \times 10^{-2}$	$3.71 \times 10^{-3}$	33.87	$3.40 \times 10^{-2}$	$4.58 \times 10^{-3}$	46.38
$\mu=0.6$	$4.69 \times 10^{-2}$	$4.94 \times 10^{-4}$	29.27	$3.69 \times 10^{-2}$	$1.35 \times 10^{-3}$	32.56	$3.16 \times 10^{-2}$	$1.92 \times 10^{-3}$	33.34	$2.80 \times 10^{-2}$	$2.26 \times 10^{-3}$	35.51
$\mu=0.4$	$5.10 \times 10^{-2}$	$3.36 \times 10^{-4}$	35.45	$3.24 \times 10^{-2}$	$6.63 \times 10^{-4}$	44.32	$2.67 \times 10^{-2}$	$8.35 \times 10^{-4}$	49.97	$2.31 \times 10^{-2}$	$9.20 \times 10^{-4}$	54.41
$\mu=0.2$	$6.65 \times 10^{-2}$	$1.31 \times 10^{-4}$	38.67	$4.59 \times 10^{-2}$	$1.99 \times 10^{-4}$	51.41	$3.61 \times 10^{-2}$	$2.23 \times 10^{-4}$	61.93	$3.04 \times 10^{-2}$	$2.28 \times 10^{-4}$	70.95

### B2. Evaluation of the proposed FOVIC model’s performance under system inertia changes

The system inertia (i.e.,  $H$ ) drops when the penetration level of RESs rises by replacing the synchronous generators, causing high-frequency deviations that may cause instability in the power system. In this case, the MG with the suggested FOVIC scheme is examined under different values of virtual inertia constant ( $K_H$ ), different values of FO operators ( $\mu$ ), and a 10% step change in load that occurs at time = 0 s. Moreover, the performance of the proposed FOVIC in the investigated system is evaluated by considering system inertia changes by  $\pm 25\%$  and  $\pm 50\%$ . Figures 17–20 show the frequency response of the

MG with system uncertainties (i.e., increasing/decreasing the system inertia by  $\pm 25\%$  and  $\pm 50\%$ , respectively). According to the results, the suggested FOVIC scheme with different values of fractional operators significantly improves the MG frequency performance. It has lower system transients compared to the integer-order VIC. Furthermore, although the frequency variation of the system with the FOVIC scheme is more suppressed when the value of the virtual inertia is increased, the system may need more time to achieve stability. Hence, the proposed FOVIC scheme still maintains the stability of the MG frequency under uncertainties (i.e., system inertia changes).

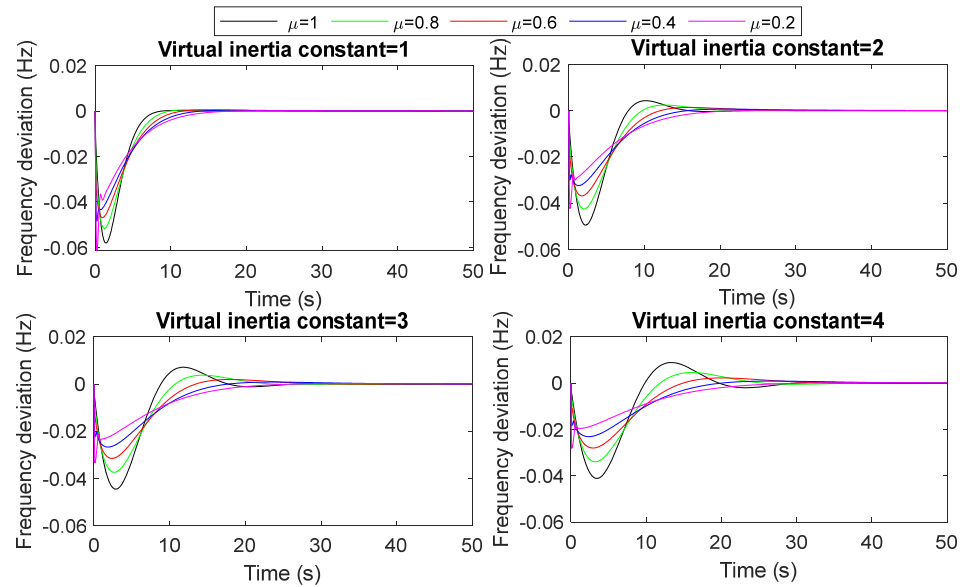


**Figure 17.** The frequency response of the MG with different values of  $K_H$  and fractional operators for case B2 with  $+25\%$  system inertia (H) variation.

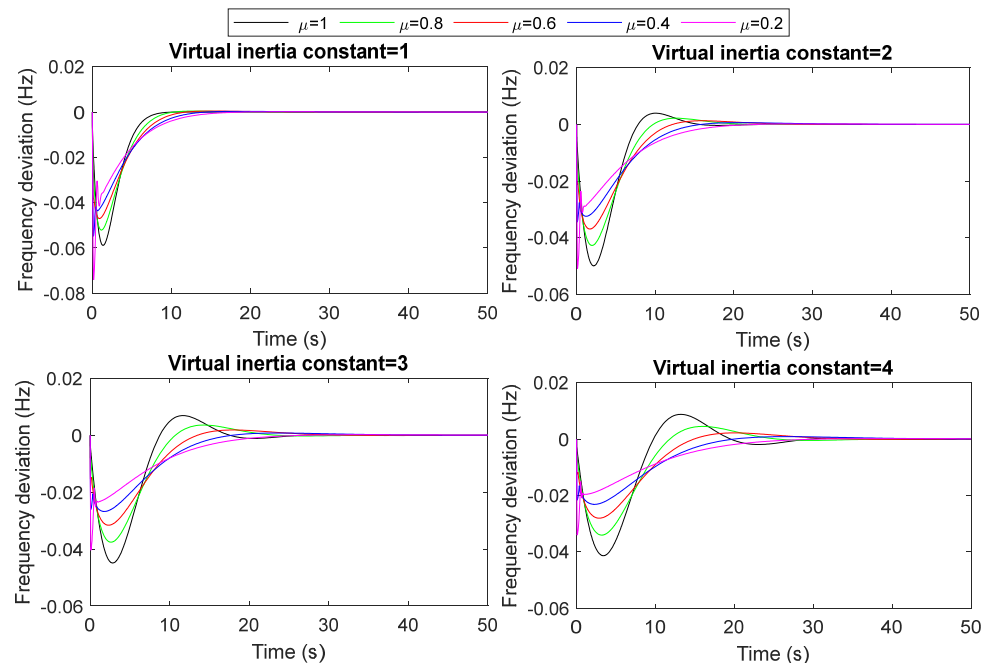


**Figure 18.** The frequency response of the MG with different values of  $K_H$  and fractional operators for case B2 with  $-25\%$  system inertia (H) variation.

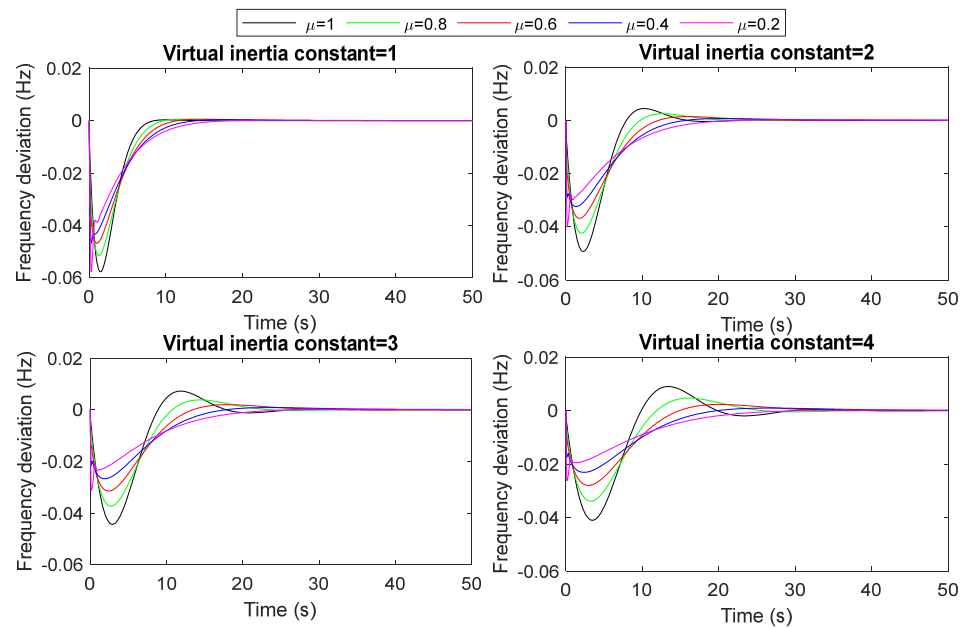


**Figure 19.** The frequency response of the MG with different values of  $K_H$  and fractional operators for case B2 with +50% system inertia (H) variation.

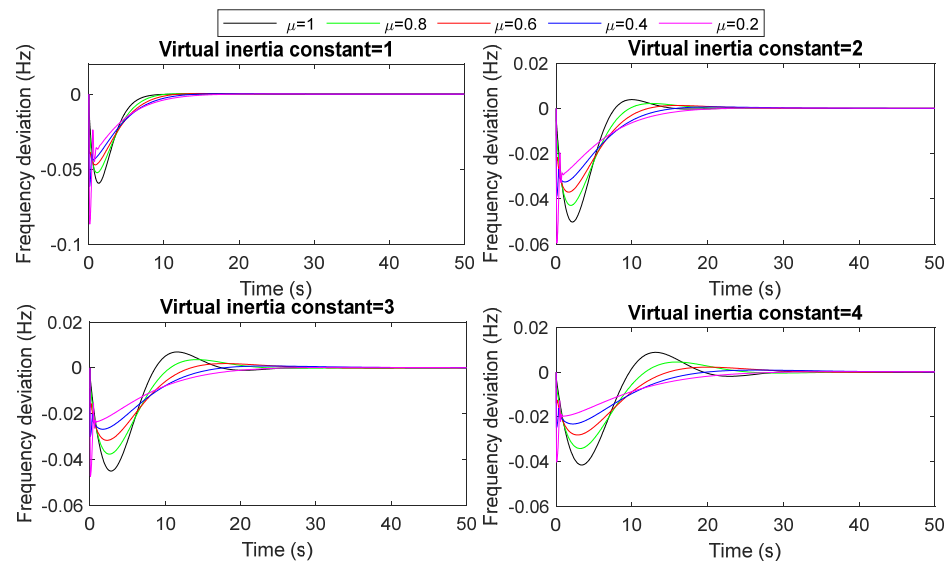


**Figure 20.** The frequency response of the MG with different values of  $K_H$  and fractional operators for case B2 with −50% system inertia (H) variation.

### B3. Evaluation of the proposed FOVIC model's performance under step load change and RESs

In this case, the MG with the suggested FOVIC scheme is investigated under different values of virtual inertia constant, different values of FO operators ( $\mu$ ), applying a series of abrupt load changes shown in Figure 21, and power fluctuations of the RESs shown in Figure 22. Figure 23 shows the frequency response of the MG with the suggested FOVIC scheme considering varied values of fractional operators. Out of the simulation results, the considered islanded MG with the proposed FOVIC scheme with different values of fractional operators is more efficient and dependable than the integer-order VIC. Additionally, compared to the proposed integer-order VIC scheme, the proposed FOVIC scheme results in a better frequency response throughout all circumstances of

this case study. Although the frequency variation of the MG with the FOVIC scheme is more suppressed when the value of  $K_H$  is increased, the system may need more time to achieve stability. Hence, the proposed FOVIC scheme still maintains the stability of the MG frequency under the high penetration of RESs.

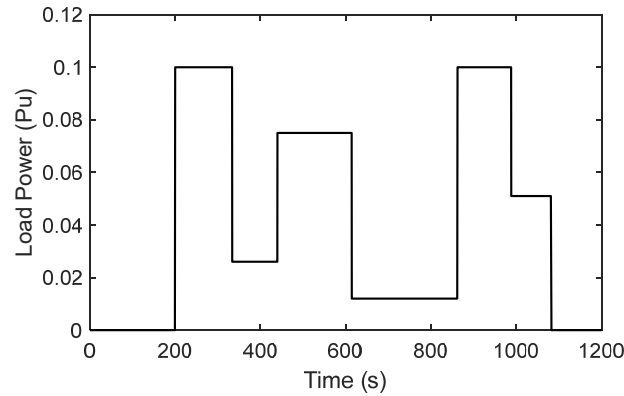


Figure 21. Load step change for case B3.

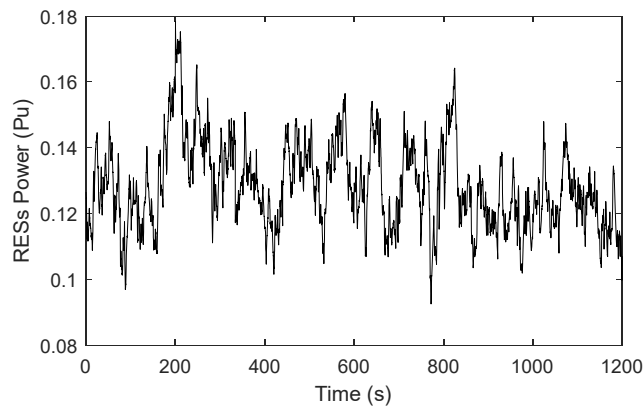


Figure 22. Renewables power generation profile for case B3.

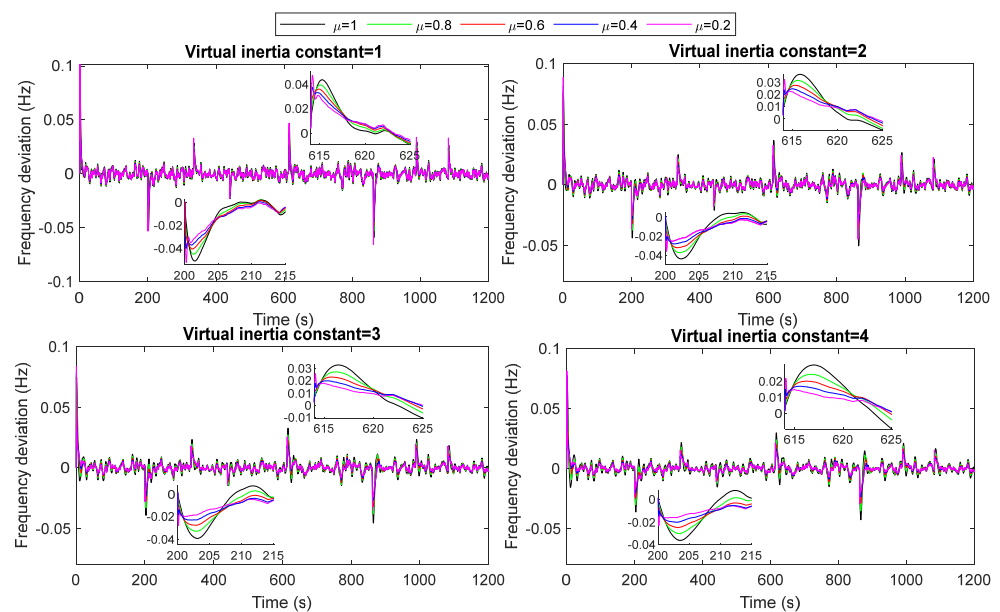


Figure 23. The frequency response of the MG with RES generation, different values of  $K_H$ , and fractional operators for case B3.

## 5. Discussion

The proposed VIC model's developed structure can provide a virtual inertia facility by controlling the battery ESS (BESS) in a way that accurately mimics the behavior of a traditional synchronous generator during the emergency period. Moreover, to provide the proposed VIC model's developed structure with more flexibility in handling various microgrid disturbances, a fractional-order derivative control has been considered. In addition to enhancing frequency response, the proposed fractional-order virtual inertia control based on the BESS permits a greater level of renewable power penetration into the microgrid. The significance of the proposed control system has been supported by the findings obtained from the previous section.

1. The proposed VIC model handles the sudden change in load demand better than the conventional VIC system by about 45% and the secondary frequency control (i.e., without VIC) system by about 80%. As a result, the proposed VIC model's developed structure has been chosen over alternative solutions for microgrid stabilization during sudden/series load changes.
2. The performance of the three control systems used—the proposed VIC model, the conventional VIC model, and the secondary load frequency control, i.e., without VIC—is evaluated under high RESs penetration as well as varying values of the system inertia constant. The system with secondary frequency control (i.e., without the VIC model) gives high oscillations that threaten the system's stability. Nonetheless, the proposed VIC and conventional VIC models are both able to stabilize the system frequency within an acceptable range. Among these two, the proposed VIC system exhibits the best frequency response under different values of the virtual inertia constant, with a maximum frequency deviation of  $\pm 0.059$  Hz (in comparison with  $\pm 0.11$  Hz by the conventional VIC system).
3. Communication time delay: With the proposed VIC model, the best frequency nadir (about 0.06 Hz) was recorded. In comparison, the conventional VIC model exhibits a frequency drop of about 0.12 Hz, whereas the load frequency control displays about 0.33 Hz. Because of this, the proposed VIC model works best in situations where there is a varying random time delay within the range of (0, 0.2), as in the case of the practical system.
4. The performance of the proposed VIC based on fractional-order derivative control has been evaluated under load/RESs fluctuations, system uncertainties (i.e., increasing/decreasing the system inertia by  $\pm 25\%$  and  $\pm 50\%$ ), and different values in the virtual inertia constant and FO operators. The results show that the microgrid with the proposed FOVIC scheme at the fractional operator equal to 0.4 is significantly more stable and faster than that designed with other fractional operator values. Furthermore, it is clear that this value falls within the range of values that were previously mentioned in the section on theoretical analysis.

## 6. Conclusions

The decreasing inertia makes modern power systems more prone to system instability. The isolated microgrids (MGs) are more susceptible to instability due to the high penetration of non-dispatchable renewable energy sources, low inertia, and small number of dispatchable generation units. Recent studies proved the efficacy of virtual inertia control (VIC) in enhancing the frequency stability of low-inertia power systems. Therefore, this study proposes a new VIC model to accurately mimic inertia power based on an energy storage system (ESS). The new VIC model considers the effect of both the DC-DC converter and the DC-AC inverter on the power of the ESS used. The obtained results prove that the proposed new VIC scheme provides fast stabilization times and slight deviations in system frequency compared to the conventional VIC schemes for all MG operating conditions and disturbances. Moreover, this study proposes a fractional-order VIC to provide greater flexibility in dealing with MG disturbances. The obtained results prove that the proposed VIC outperforms the conventional LFC by about 80% and the conventional VIC model

by about 45% in tackling loads/RESs fluctuations and system uncertainty. Hence, the proposed FOVIC scheme is noticeably more stable and faster in response compared to that designed with integer-order VIC for all MG operating conditions and disturbances.

**Author Contributions:** Conceptualization, M.N., G.M., A.B. (Abualkasim Bakeer) and H.A.; methodology, M.N., G.M., A.B. (Abualkasim Bakeer) and H.A.; software, M.N., G.M. and A.B. (Abualkasim Bakeer); validation, M.N., G.M. and A.B. (Abualkasim Bakeer); formal analysis, M.N., G.M., A.B. (Abualkasim Bakeer) and H.A.; investigation, M.N., G.M., A.B. (Abualkasim Bakeer) and H.A.; resources, M.N., G.M., A.B. (Abualkasim Bakeer) and H.A.; data curation, M.N., G.M., A.B. (Abualkasim Bakeer) and H.A.; writing—original draft preparation, M.N., G.M., A.B. (Abualkasim Bakeer) and H.A.; writing—review and editing, M.N., G.M., A.B. (Abualkasim Bakeer), A.A.T., A.B. (Abderrahmane Beroual), U.K. and H.A.; visualization, M.N., G.M. and A.B. (Abualkasim Bakeer); supervision, A.A.T., A.B. (Abderrahmane Beroual) and U.K.; project administration, A.A.T., A.B. (Abderrahmane Beroual) and U.K.; funding acquisition, A.A.T. and U.K. All authors have read and agreed to the published version of the manuscript.

**Funding:** This work was supported by the Researchers Supporting Program number (RSPD2023R1108), King Saud University, Riyadh, Saudi Arabia.

**Data Availability Statement:** Data are available on request from the authors.

**Acknowledgments:** The authors present their appreciation to King Saud University for funding this research through Researchers Supporting Program Number (RSPD2023R1108), King Saud University, Riyadh, Saudi Arabia.

**Conflicts of Interest:** The authors declare no conflict of interest.

## References

1. International Renewable Energy Agency (IRENA). *Global Energy Transformation: A Roadmap to 2050*; IRENA: Masdar City, United Arab Emirates, 2019.
2. Magdy, G.; Nour, M.; Shabib, G.; Elbaset, A.A.; Mitani, Y. Supplementary Frequency Control in a High-Penetration Real Power System by Renewables Using SMES Application Electrical Systems. *J. Electr. Syst.* **2019**, *15*, 526–538.
3. Dreidy, M.; Mokhlis, H.; Mekhilef, S. Inertia response and frequency control techniques for renewable energy sources: A review. *Renew. Sustain. Energy Rev.* **2017**, *69*, 144–155. [[CrossRef](#)]
4. Fathi, A.; Shafiee, Q.; Bevrani, H. Robust Frequency Control of Microgrids Using an Extended Virtual Synchronous Generator. *IEEE Trans. Power Syst.* **2018**, *33*, 6289–6297. [[CrossRef](#)]
5. Peng, Q.; Jiang, Q.; Yang, Y.; Liu, T.; Wang, H.; Blaabjerg, F. On the Stability of Power Electronics-Dominated Systems: Challenges and Potential Solutions. *IEEE Trans. Ind. Appl.* **2019**, *55*, 7657–7670. [[CrossRef](#)]
6. Ulbig, A.; Borsche, T.S.; Andersson, G. Impact of Low Rotational Inertia on Power System Stability and Operation. *IFAC Proc. Vol.* **2014**, *19*, 7290–7297. [[CrossRef](#)]
7. Santurino, P.; Sigrist, L.; Ortega, Á.; Renedo, J.; Lobato, E. Optimal coordinated design of under-frequency load shedding and energy storage systems. *Electr. Power Syst. Res.* **2022**, *211*, 108423. [[CrossRef](#)]
8. Ranjan, M.; Shankar, R. A literature survey on load frequency control considering renewable energy integration in power system: Recent trends and future prospects. *J. Energy Storage* **2022**, *45*, 103717. [[CrossRef](#)]
9. Makolo, P.; Zamora, R.; Lie, T.-T. The role of inertia for grid flexibility under high penetration of variable renewables—A review of challenges and solutions. *Renew. Sustain. Energy Rev.* **2021**, *147*, 111223. [[CrossRef](#)]
10. Mohanty, B.; Hota, P.K. Comparative performance analysis of fruit fly optimisation algorithm for multi-area multi-source automatic generation control under deregulated environment. *IET Gener. Transm. Distrib.* **2015**, *9*, 1845–1855. [[CrossRef](#)]
11. El-Sousy, F.F.M.; Aly, M.; Alqahtani, M.H.; Aljumah, A.S.; Almutairi, S.Z.; Mohamed, E.A. New Cascaded 1+PII2D/FOPID Load Frequency Controller for Modern Power Grids including Superconducting Magnetic Energy Storage and Renewable Energy. *Fractal Fract.* **2023**, *7*, 672. [[CrossRef](#)]
12. Shayeghi, H.; Rahnama, A.; Bizon, N. TFODn-FOPI multi-stage controller design to maintain an islanded microgrid load-frequency balance considering responsive loads support. *IET Gener. Transm. Distrib.* **2023**, *17*, 3266–3285. [[CrossRef](#)]
13. Peddakapu, K.; Srinivasarao, P.; Mohamed, M.; Arya, Y.; Kishore, D.K. Stabilization of frequency in Multi-Microgrid system using barnacle mating Optimizer-based cascade controllers. *Energy Technol. Assess.* **2022**, *54*, 102823. [[CrossRef](#)]
14. Sahu, P.C.; Jena, S.; Mohapatra, S.; Debdas, S. Impact of energy storage devices on microgrid frequency performance: A robust DQN based grade-2 fuzzy cascaded controller. *e-Prime* **2023**, *6*, 100288. [[CrossRef](#)]
15. Ali, H.; Li, B.; Xu, Z.; Liu, H.; Xu, D. Virtual Synchronous Generator Design Based Modular Multilevel Converter for Microgrid Frequency Regulation. In Proceedings of the 2019 22nd International Conference on Electrical Machines and Systems (ICEMS), Harbin, China, 11–14 August 2019; Volume 1, pp. 1–6.



16. Zhong, Q.-C.; Weiss, G. Synchronverters: Inverters that mimic synchronous generators. *IEEE Trans. Ind. Electron.* **2011**, *58*, 1259–1267. [[CrossRef](#)]
17. Fang, J.; Li, H.; Tang, Y.; Blaabjerg, F. Distributed Power System Virtual Inertia Implemented by Grid-Connected Power Converters. *IEEE Trans. Power Electron.* **2018**, *33*, 8488–8499. [[CrossRef](#)]
18. Nour, M.; Magdy, G.; Chaves-Ávila, J.P.; Sánchez-Miralles, A.; Jurado, F. A new two-stage controller design for frequency regulation of low-inertia power system with virtual synchronous generator. *J. Energy Storage* **2023**, *62*, 106952. [[CrossRef](#)]
19. Mohammadi-ivatloo, B. Provision of Frequency Stability of an Islanded Microgrid Cascade Controller. *Energies* **2021**, *14*, 4152.
20. Magdy, G.; Shabib, G.; Elbaset, A.A.; Mitani, Y. A Novel Coordination Scheme of Virtual Inertia Control and Digital Protection for Microgrid Dynamic Security Considering High Renewable Energy Penetration. *IET Renew. Power Gener.* **2019**, *13*, 462–474. [[CrossRef](#)]
21. Gonzalez-Longatt, F.; Chikuni, E.; Rashayi, E. Effects of the Synthetic Inertia from wind power on the total system inertia after a frequency disturbance. In Proceedings of the 2013 IEEE International Conference on Industrial Technology (ICIT), Cape Town, South Africa, 25–28 February 2013; pp. 826–832.
22. Hu, Y.; Wei, W.; Peng, Y.; Lei, J. Fuzzy virtual inertia control for virtual synchronous generator. *Chinese Control Conf. CCC* **2016**, *2016*, 8523–8527.
23. Magnus, D.M.; Scharlau, C.C.; Pfitscher, L.L.; Costa, G.C.; Silva, G.M. A novel approach for robust control design of hidden synthetic inertia for variable speed wind turbines. *Electr. Power Syst. Res.* **2021**, *196*, 107267. [[CrossRef](#)]
24. Ali, H.; Magdy, G.; Li, B.; Shabib, G.; Elbaset, A.A.; Xu, D.; Mitani, Y. A New Frequency Control Strategy in an Islanded Microgrid Using Virtual Inertia Control-Based Coefficient Diagram Method. *IEEE Access* **2019**, *7*, 16979–16990. [[CrossRef](#)]
25. Sockeel, N.; Gafford, J.; Papari, B.; Mazzola, M. Virtual Inertia Emulator-Based Model Predictive Control for Grid Frequency Regulation Considering High Penetration of Inverter-Based Energy Storage System. *IEEE Trans. Sustain. Energy* **2020**, *11*, 2932–2939. [[CrossRef](#)]
26. Li, J.; Wen, B.; Wang, H. Adaptive Virtual Inertia Control Strategy of VSG for Micro-Grid Based on Improved Bang-Bang Control Strategy. *IEEE Access* **2019**, *7*, 39509–39514. [[CrossRef](#)]
27. Fawzy, A.; Bakeer, A.; Magdy, G.; Atawi, I.E.; Roshdy, M. Adaptive Virtual Inertia-Damping System Based on Model Predictive Control for Low-Inertia Microgrids. *IEEE Access* **2021**, *9*, 109718–109731. [[CrossRef](#)]
28. Alipoor, J.; Miura, Y.; Ise, T. Stability Assessment and Optimization Methods for Microgrid with Multiple VSG Units. *IEEE Trans. Smart Grid* **2016**, *9*, 1462–1471. [[CrossRef](#)]
29. Padhy, S.; Panda, S. Simplified grey wolf optimisation algorithm tuned adaptive fuzzy PID controller for frequency regulation of interconnected power systems. *Int. J. Ambient. Energy* **2022**, *43*, 4089–4101. [[CrossRef](#)]
30. Ali, H.; Magdy, G.; Xu, D. A new optimal robust controller for frequency stability of interconnected hybrid microgrids considering non-inertia sources and uncertainties. *Int. J. Electr. Power Energy Syst.* **2021**, *128*, 106651. [[CrossRef](#)]
31. Liu, J.; Yang, Z.; Yu, J.; Huang, J.; Li, W. Coordinated control parameter setting of DFIG wind farms with virtual inertia control. *Int. J. Electr. Power Energy Syst.* **2020**, *122*, 106167. [[CrossRef](#)]
32. Fini, M.H.; Golshan, M.E.H. Determining optimal virtual inertia and frequency control parameters to preserve the frequency stability in islanded microgrids with high penetration of renewables. *Electr. Power Syst. Res.* **2018**, *154*, 13–22. [[CrossRef](#)]
33. Mohamed Mostafa Elsaied, H.M.H.; Hameed, W.H.A. Frequency stabilization of a hybrid three-area power system equipped with energy. *IET Renew. Power Gener.* **2022**, *16*, 3267–3286. [[CrossRef](#)]
34. Alilou, M.; Azami, H.; Oshnoei, A.; Mohammadi-Ivatloo, B.; Teodorescu, R. Fractional-Order Control Techniques for Renewable Energy and Energy-Storage-Integrated Power Systems: A Review. *Fractal Fract.* **2023**, *7*, 391. [[CrossRef](#)]
35. Pan, I.; Das, S. Kriging Based Surrogate Modeling for Fractional Order Control of Microgrids. *IEEE Trans. Smart Grid* **2015**, *6*, 36–44. [[CrossRef](#)]
36. Monje, A.; Chen, Y.; Vinagre, B.M.; Xue, D.; Feliu, V. *Fractional Order Systems and Controls*; Springer: Berlin/Heidelberg, Germany, 2010.
37. Debbarma, S.; Saikia, L.C.; Sinha, N. AGC of a multi-area thermal system under deregulated environment using a non-integer controller. *Electr. Power Syst. Res.* **2013**, *95*, 175–183. [[CrossRef](#)]
38. Saxena, S. Load frequency control strategy via fractional-order controller and reduced-order modeling. *Int. J. Electr. Power Energy Syst.* **2019**, *104*, 603–614. [[CrossRef](#)]
39. Pan, I.; Das, S. Fractional Order AGC for Distributed Energy Resources Using Robust Optimization. *IEEE Trans. Smart Grid* **2015**, *7*, 2175–2186. [[CrossRef](#)]
40. Nour, M.; Magdy, G.; Chaves-Avila, J.P.; Sanchez-Miralles, A.; Petlenkov, E. Automatic Generation Control of a Future Multisource Power System Considering High Renewables Penetration and Electric Vehicles: Egyptian Power System in 2035. *IEEE Access* **2022**, *10*, 51662–51681. [[CrossRef](#)]
41. Yu, Y.; Guan, Y.; Kang, W.; Chaudhary, S.K.; Vasquez, J.C.; Guerrero, J.M. Fractional-Order Virtual Synchronous Generator. *IEEE Trans. Power Electron.* **2023**, *38*, 6874–6879. [[CrossRef](#)]
42. Long, B.; Li, X.; Rodriguez, J.; Guerrero, J.M.; Chong, K.T. Frequency stability enhancement of an islanded microgrid: A fractional-order virtual synchronous generator. *Int. J. Electr. Power Energy Syst.* **2023**, *147*. [[CrossRef](#)]
43. Morsali, J.; Zare, K.; Hagh, M.T. Applying fractional order PID to design TCSC-based damping controller in coordination with automatic generation control of interconnected multi-source power system. *Eng. Sci. Technol. Int. J.* **2017**, *20*, 1–17. [[CrossRef](#)]

44. Podlubny, I. *Fractional Differential Equations: An Introduction to Fractional Derivatives, Fractional Differential Equations, to Methods of Their Solution and Some of Their Applications*; Elsevier: Amsterdam, The Netherlands, 1998.
45. Moschos, I.; Parisses, C. A novel optimal PIADND2N2 controller using coyote optimization algorithm for an AVR system. *Eng. Sci. Technol. Int. J.* **2022**, *26*, 100991. [[CrossRef](#)]
46. Kerdphol, T.; Rahman, F.S.; Watanabe, M.; Mitani, Y. *Virtual Inertia Synthesis and Control*; Springer: Dordrecht, The Netherlands, 2021.

**Disclaimer/Publisher's Note:** The statements, opinions and data contained in all publications are solely those of the individual author(s) and contributor(s) and not of MDPI and/or the editor(s). MDPI and/or the editor(s) disclaim responsibility for any injury to people or property resulting from any ideas, methods, instructions or products referred to in the content.